Temperature dependence of magnetic coupling in ultrathin NiO/Fe_3O_4(001) films

C. Boeglin,* O. Ersen, M. Pilard, and V. Speisser
Institut de Physique et de Chimie de Strasbourg, Université Louis Pasteur, CNRS UMR 7504, 23 rue du Loess, 67034 Strasbourg, France

F. Kronast
BESSY, Albert-Einstein-Strasse 15, 12489 Berlin, Germany

(Received 15 January 2009; revised manuscript received 9 April 2009; published 9 July 2009)

We have studied the evolution of nanometer-sized magnetic domains in exchange-coupled NiO/Fe_3O_4(001) bilayers as a function of temperature. To image magnetic domains in thin antiferromagnetic (AF) NiO and in ferrimagnetic (FM) Fe_3O_4(001) layers we have used element specific x-ray photoemission electron microscopy. The epitaxial growth of NiO/Fe_3O_4(001) leads to a parallel orientation between the two oxide lattices. The magnetic order-disorder transition temperature of a 2-nm-NiO/Fe_3O_4(001) film is found to be T_N =375 K, much lower than for bulk NiO (T_N=520 K). Setting the temperature below or above the Néel temperature (T_N) of ultrathin NiO films, the influence of the interlayer exchange coupling on the microscopic domain patterns could be studied. Below T_N, the two layers reveal parallel coupling and an induced twofold degenerated spin configuration. Small nanometer domains are observed inside the larger micrometer magnetic domain of Fe_3O_4(001). Alternating direction of the spins, pointing along ⟨100⟩ and ⟨120⟩ are present in both the AF and FM layers. Above T_N, the AF contrast in the magnetic image of NiO vanishes and simultaneously large micrometer magnetic domains appear in Fe_3O_4(001), showing magnetic contrast images of uncoupled spins oriented parallel to ⟨100⟩. The consequences of the microscopic magnetic domain patterns in FM/AF coupled systems are discussed in terms of macroscopic magnetic properties.

DOI: 10.1103/PhysRevB.80.035409 PACS number(s): 75.70.Kw, 75.50.Ee, 75.70.Cn, 75.70.Rf

I. INTRODUCTION

The magnetic coupling between ferro(i)magnetic (FM) and antiferromagnetic (AF) materials is nowadays a widely studied phenomenon in the field of magnetism. This is due to technological challenges facing exchange-coupled metal/oxide devices.[1] The motivation behind that is related to the still controversial mechanism of exchange bias used in magnetic spin valves, for instance. Realistic models for the magnetic exchange coupling at FM/AF interfaces may significantly deviate from bulk configurations. Recently, important progresses were made in order to model these interfaces. A large number of investigations have been performed concerning the surfaces of oxides[2,3] and films deposited on metal single crystals[4] as well as the electronic[5–10] and crystal structures of oxides.[11–13] In recent times, x-ray magnetic linear dichroism has been offering a direct characterization of the AF order in thin films as a complement to neutron-diffraction experiments that are restricted to rather large amounts of materials.[14,15] Compared to bulk NiO, thin films are expected to show different antiferromagnetic properties. For instance, strains and defects are expected to be different in both systems, as recently demonstrated by Csiszar *et al.*[16] in strained CoO films. As far as magnetism is concerned, the induced spin planes and spin orientations in these strained AF films are changed with respect to the bulk.

In this framework, the coupling between NiO and adjacent metals has been extensively studied using NiO(100) single crystals and thin films[17–20] and reflects the importance of the defects and chemical reduction in the metal/oxide interfaces or of the atomic steps favoring uncompensated magnetic moments at the interface which are thought to be at the origin of less efficient magnetic coupling.[17,18,20–25] Alternatively, NiO films were grown on oxide substrates, preventing chemical reduction.[20,26,27] The presence of a spinel structure at the NiO/Fe_3O_4(001) interface has a direct influence on the coupling.[20] Depending on the system studied, different magnetic couplings were found. Parallel coupling was demonstrated in NiO/Fe_3O_4(001) (Ref. 20) and NiO/Fe_3O_4(110) (Ref. 28) whereas perpendicular coupling was observed in NiO/Fe(100) films[21,24] and in Co/NiO(001).[17,18,29] The magnetic coupling is obviously mainly related to the interface compound (defined by structural and chemical aspects) formed by the epitaxial growth. On the micrometer scale, large domain configurations can be observed for different growth directions of NiO/Fe_3O_4.[20,28] Several authors studied the question of the driving force behind the magnetic coupling in this system but they reached different conclusions.[18,20,28] Some of them argue that the magnetic coupling is determined by the amount of uncompensated spins at the interface, others claim that the interface magnetocrystalline anisotropy or the interface crystalline orientations are the most important parameters controlling the magnetic coupling. The controversy initiated by those experiments on AF/FM layers shows that the driving force of the magnetic coupling is still not elucidated at the microscopic level. At this point, a more detailed description of the nanometer magnetic domain structures is called for and will here allow us to have a closer look at the micromagnetic configuration of coupled and uncoupled NiO/Fe_3O_4(001) layers in order to determine the origin of the coupling mechanism in this system. This is now possible through high-resolution photoemission electron microscopy (PEEM) experiments where the influence of the magnetic coupling can be studied directly on the magnetic domains structure using temperature variations through the critical temperature

of the magnetic ordering of one of the layers. The effect and the consequences of such microscopic magnetic domains in FM/AF coupled systems will be elucidated here. Especially, we will be able to define the real-domain sizes and the orientations of the spins in both layers, as well as to gauge the influence of the Néel temperature (T_N) in ultrathin NiO films, questions which were never addressed before. Finally, we will resolve the micromagnetic origin of the averaged spin direction and of the lower magnetic moments observed for coupled $NiO/Fe_3O_4(001)$ layers, arising from averaging measurements in the micrometer range.

II. EXPERIMENT

We have studied the magnetic interlayer coupling of ultrathin NiO films grown on $Fe_3O_4(001)$ on the nanometer scale using x-ray photoelectron emission microscopy (X-PEEM). We have imaged the evolution of nanometer-sized magnetic domains in this exchange-coupled FM/AF system as a function of temperature, whereby the magnetic coupling could be switched on and off by going through the Néel temperature (T_N) of the ultrathin NiO film.

Ultrathin 2-nm-thick NiO films were grown on $Fe_3O_4(001)$ at 610 K as described by Pilard *et al.*[20] Magnetic imaging was performed using the SPEEM endstation at the UE49PGMa beamline of the BESSY Synchrotron facility in Berlin. The SPEEM setup is based on a conventional Elmitec PEEM providing a lateral resolution of about 30 nm using x-ray excitation. The incidence angle of the incoming x-ray beam was fixed at 74°. To obtain element-specific domain images in PEEM we exploited the x-ray magnetic circular dichroism (XMCD) and the x-ray magnetic linear dichroism (XMLD) contrasts at the Fe $L_{2,3}$ and Ni $L_{2,3}$ edges, respectively. For XMCD measurements, the beamline provided circular polarized light with a degree of polarization of about 90%. XMLD measurements were performed using linear polarized x-ray with the electric vector E in the plane of the sample.

Previous results published by Pilard *et al.*[20] showed that all the spins present in NiO and $Fe_3O_4(001)$ are oriented collinear and aligned in-plane along the ⟨100⟩ directions. For the sample studied in this paper, this particular orientation was confirmed by performing angular-dependent measurements at room temperature using the PEEM imaging mode. The linear polarization vector of the x-ray beam has been rotated from the in-plane to out-of-plane direction in order to exclude a possible out-of-plane orientation of the NiO spins. A detailed description of this angular analysis will be published in a forthcoming paper.

In this work, due to the presence of the cooling system, the sample holder could not be rotated during the temperature-dependent measurements. An individual series of images has been recorded at a different location on the surface of the sample at room temperature allowing performing a complete azimuth angular dependence of the XMCD at the Fe L_3 edge and XMLD at the Ni L_2 edges. From these images, a quantitative analysis of the magnetic contrast has been performed using the angular dependence of the contrast in the PEEM images. The two angular-dependences $\cos(\varphi)$ and $\cos^2(\varphi)$ corresponding to, respectively, the XMCD and the XMLD intensities were found, allowing us to determine the orientation of magnetic moments in the surface of the film. The XMCD intensity for Fe_3O_4 ranges from −12% to +12%. The XMLD intensity R, obtained for NiO, ranges from 0.89 to 1.15. All these numerical values are coherent to the measured values obtained for thin $NiO/Fe_3O_4(001)$ films as described by Pilard *et al.*[20] We orient the sample in-plane direction [100] along the incident light direction.

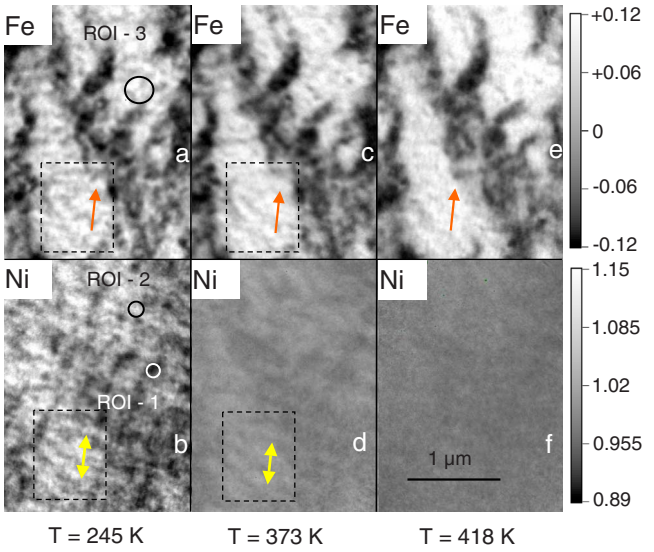

FIG. 1. (Color online) Magnetic contrast images obtained using XMC(L)D-PEEM, at the Fe L_3 edge [top images; (a), (c), and (e)] and Ni L_2 edge [bottom images; (b), (d), and (f)] showing the magnetic domains in the ferrimagnetic $Fe_3O_4(001)$ substrate and in the 2 nm AF NiO film at sample temperatures of T=245, 373, and 418 K. The size of the images is 2×3 μm^2. Circles indicate the regions of interest (ROI) corresponding to the energy spectra in Fig. 2. The scale bar for the Fe L_3-edge images provides normalized XMCD values. The scale bar for the Ni L_2-edge images provides the ratio between the low-energy (LE) and the high-energy (HE) peak intensities at the Ni L_2 edge [Fig. 2(a)]. These values are coherent with those measured by Pilard *et al.* (Ref. 20) for $NiO/Fe_3O_4(001)$ ultrathin films.

III. RESULTS

A. Temperature-dependent magnetic imaging

In order to follow the evolution with temperature of the FM domains in $Fe_3O_4(001)$ and of the AF domains in the thin NiO films we have systematically compared the XMCD-PEEM images recorded at the Fe L_3 edge [Figs. 1(a), 1(c), and 1(e)] with the XMLD-PEEM images recorded at the Ni L_2 edge [Figs. 1(b), 1(d), and 1(f)]. In Fig. 1, one can compare the FM domains in $Fe_3O_4(001)$ to the AF domains in a 2-nm-thick NiO film. The magnetic contrast images show a specific sample area of 2 micrometer $\times3$ micrometer recorded at temperatures of 245, 373, and 418 K, never exceeding the growth temperature of 610 K. The NiO-XMLD images are obtained by calculating the ratio between the low-energy (LE) and the high-energy (HE) peak

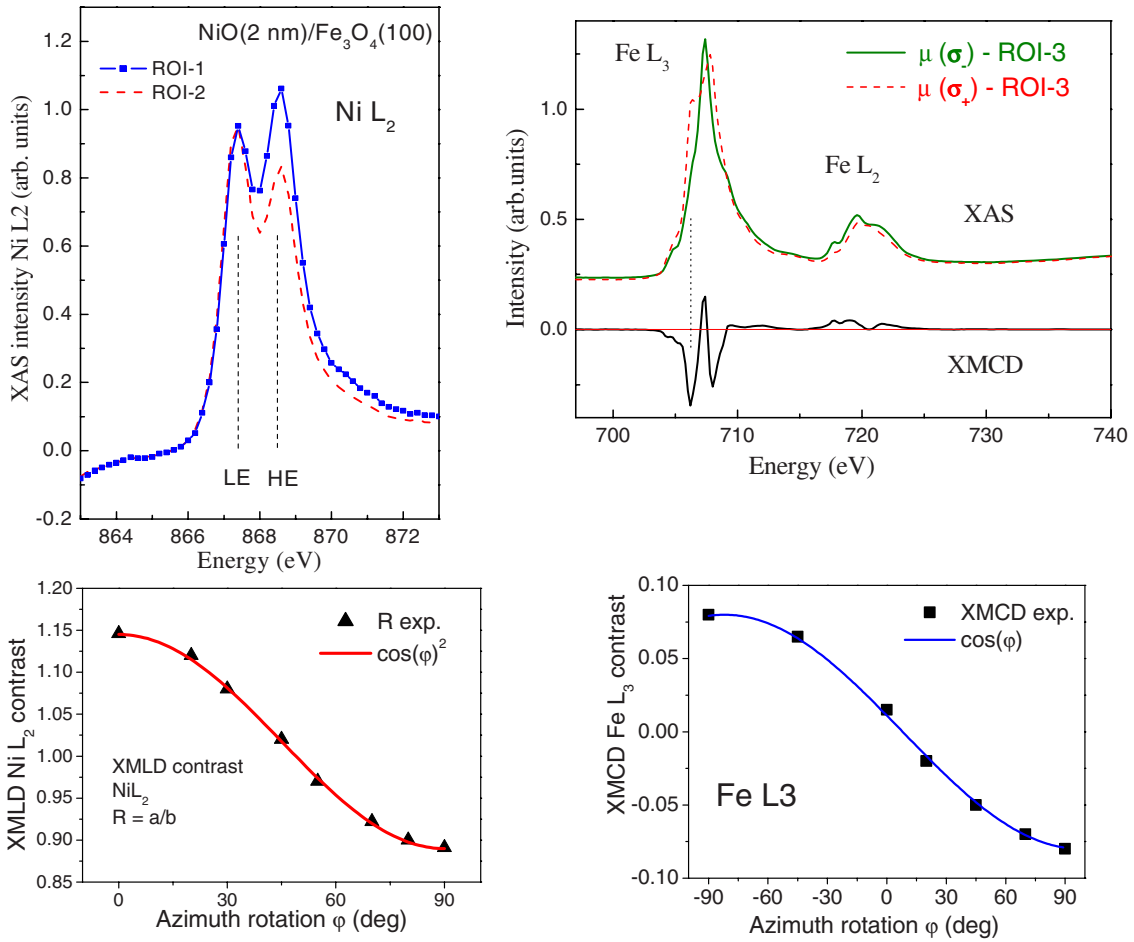

FIG. 2. (Color online) Local microspectra taken for the 2-nm-NiO/Fe_3O_4(001) film at the Ni L_2 and Fe $L_{2,3}$ edges and extracted from the region of interest (ROI) 1, 2, and 3 in the magnetic contrast images in Fig. 1(a) and Fig. 1(b). The XMCD obtained at the Fe $L_{2,3}$ edges determine the energy which was used to image the FM domains in Fe_3O_4. Below each microspectra we present the fits of the angular dependences of the polarization in the XMLD Ni L_2 (left) and in the XMCD Fe L_3 (right).

intensities at the Ni L_2 edge [Fig. 2(a)]. The Fe_3O_4(001)-XMCD images are obtained from the normalized difference between the two images taken with opposite circular polarization at the Fe L_3 edge corresponding to the octahedral site of Fe_3O_4 at the lowest energy of the Fe L_3 edge [Fig. 2(b)]. The microspectra shown in Fig. 2 are extracted from the region of interest (ROI) in the magnetic contrast images in Figs. 1(a) and 1(b).

The image obtained by XMCD-PEEM at the Fe L_3 edge at $T=245$ K and 373 K is white-gray contrasted inside one of the large micrometer domains (dashed area). The major difference between the Ni L_2 and Fe L_3 magnetic image contrasts in this dashed area, results from the different contrast techniques used in XMLD and XMCD. The first-image technique leads to a 180° color symmetry whereas XMCD shows a 360° symmetry. In other words, corresponding to the Fe_3O_4 white-gray contrast in the dashed area of Fig. 1(a) we observe a white-dark contrast in the NiO image [Fig. 1(b)]. Although above $T=300$ K, we can observe a temperature evolution in the XMCD magnetic contrast of the FM layer [Figs. 1(c) and 1(e)] that is somewhat harder to distinguish as compared to the corresponding one in the AF layer NiO [Figs. 1(d) and 1(f)]. In order to confirm the parallel and coherent magnetic contrast decrease with temperature in the FM and AF nanometer domains, we had to extract and follow the evolutions of the quantitative values of the XMLD and XMCD contrasts. This will be presented in the last section.

When cycling the temperature between $T=150$ and $T=460$ K, the changes in the Fe_3O_4 layer are completely reversible, confirming that the maximum temperature used does not change the chemistry and the defects located at the NiO/Fe_3O_4(001) interface. The influence of cycling the sample temperature between 150 and 460 K is limited to magnetic-domain training effects[30] observed, for instance, at the right side of the white triangular domain [Fig. 1(e)]. Such limited (<5%) effects are probably related to the switching of unstable as-grown micrometer domains at the interface. This is probably related to the instability of the interface magnetization of the AF pinning layer as suggested by Binek *et al.*[30] We will discuss this point in more detail in the last section. Once established, the domain structure does not change further even after several temperature cycling. In Fig. 1(e), we present the final configuration of the Fe_3O_4(001) magnetic contrast image. Concerning the nanometer domains induced by the coupling with NiO, we have to notice that,

after each excursion to $T > T_N$, the fine structure of those nanometer magnetic domains at $T=150$ K is different. This indicates that the configuration of the nanometer-sized domains is strongly related to exchange-coupling energy which couples NiO with $Fe_3O_4(001)$ in the vicinity of the interface.

As a first step, we will present a qualitative description of the magnetic-domain pattern in NiO and $Fe_3O_4(001)$ films as a function of the temperature. At low temperature [Fig. 1(b)—$T<245$ K], the AF contrast in the NiO layer is important, showing small nanometer magnetic patterns. Increasing the temperature, we observe a progressive decrease in the AF contrast in the NiO layer [Fig. 1(e)] strongly reduced at $T=418$ K [Fig. 1(f)]. This indicates a continuous phase transition in the ultrathin NiO film. Above 418 K, a further increase in temperature to 460 K does not yield any change in magnetic contrast for the NiO layer. At the temperature of $T=373$ K, the AF film is close to $T=T_N$. The magnetic order is weakened but, in Fig. 1(d), we still observe nanometer-sized magnetic contrast areas at the Ni L_2 edge. The transition between Figs. 1(d) and 1(f) is here obvious because the magnetically disordered state is reached in NiO at $T=418$ K. The changes in contrast with temperature correspond to a second-order phase transition at $T=T_N$ as will be quantitatively derived from the magnetic contrast images in the last section.

In the magnetic images obtained for the $Fe_3O_4(001)$ substrate, we show that, below T_N, [Fig. 1(a)—$T=245$ K] the FM layer shows large micrometer-sized FM domains superimposed by a pattern of smaller magnetic domains with an average size of about 100 nm. These superimposed nanometer pattern in the FM layer disappears above T_N. We also observe that, in the temperature range 200–350 K, the contrast obtained from the nanometer domains inside each larger micrometer domain in $Fe_3O_4(001)$ is high whereas it becomes very weak above $T=350$ K. However, the large micrometer-sized magnetic domains do not show strong variations with temperature. The micrometer-sized FM domains in $Fe_3O_4(001)$ transform during the temperature increase to a more and more homogenous contrast.

Finally, the superimposed patterns of nanometer- and micrometer-sized FM domains in $Fe_3O_4(001)$ only appear at low temperature [Figs. 1(a) and 1(c)] when the AF order is present in NiO. This is a first evidence of the coupling with the NiO magnetic-domain pattern. At $T=413$ K the large magnetic domains in $Fe_3O_4(001)$ present spins oriented along the two equivalent in-plane ⟨100⟩ directions (see experimental section and color bars). The domain walls are chiefly aligned parallel to ⟨110⟩ directions.

In order to compare the local domain configuration in NiO and $Fe_3O_4(001)$, we make a quantitative analysis in restricted areas of the magnetic contrast images. To compare the nanometer magnetic domains in the FM and AF film at low temperature, we have to take into account that the XMLD and XMCD contrasts are different, so that on the bases of Figs. 1(a) and 1(b) we can readily conclude to a coherent superposition of both local domains. In order to compare the two contrast images (XMLD and XMCD) we have to restrict our attention to specific areas shown in Fig. 3 as a square zone extracted from the bottom part of the images in Fig. 1 (dashed area). We restricted the scale only to a

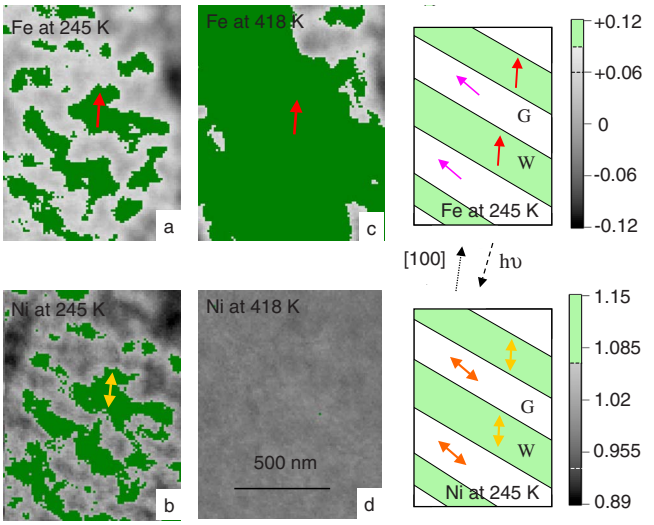

FIG. 3. (Color online) Magnetic-domain images at $T=245$ K and $T=418$ K in $Fe_3O_4(001)$ and in the NiO film. The images are extracted from the red dashed area shown in Fig. 1. The same scale bars are used as in Fig. 1. The images are green colored by selecting the local nm magnetic domains with spins parallel to [100]. The green selected domains (W) correspond to the XMCD values ranging from 0.12 to 0.09 whereas the G domains, still in gray, correspond to the XMCD values ranging from 0.09 to 0.06. The selected zone is schematically drawn at the right side in order to show the successive G and W domains in both FM and AF layers at $T=245$ K. The magnetic images obtained at $T=418$ K show that a homogenous green color is obtained (single domain) in $Fe_3O_4(001)$ whereas in NiO the magnetic contrast has disappeared. The scale of the magnetic images is 1×1.2 μm^2.

single micrometer magnetic domain so that the simplest case of magnetic contrast can be observed. In Fig. 3, we have highlighted a set of magnetic images recorded at $T=245$ and $T=418$ K where the green domains show spins parallel to [100]. This result is obtained after a quantitative analysis of the magnetic contrast, which allows us to determine the orientation of magnetic moments with a high accuracy as explained in the experimental section. As sketched in the right part of Fig. 3, we can represent the alternating domains at $T=245$ K for NiO and for $Fe_3O_4(001)$. Selecting in the magnetic images of Fig. 3 the spins parallel to [100], we can easily compare the FM domains in $Fe_3O_4(001)$ with the AF domain pattern in the NiO film. Moreover, the signal-to-noise ratio is larger in the NiO magnetic contrast images that enlarge the green areas in the AF film. Despite these differences, one observes that any of the FM domains in $Fe_3O_4(001)$ shows a correspondent AF domain in the NiO film.

Inside the single domain in $Fe_3O_4(001)$ [Fig. 3(a)], one can observe that the green selected domains are separated by domains where the spins are differently oriented. In this zone, the quantitative analysis of the magnetic contrast shows that the spins are successively oriented along the in-plane [100] direction and $\pm60°$ off this direction. These two types of magnetic domains will be called in the following W (white contrast) and G (gray contrast), respectively. The $\pm60°$ directions approximately correspond to in-plane ⟨210⟩ directions.

In order to estimate if the measured XMCD signal is an average through several magnetite layers, in particular a result of a mixing of coupled (near the interface) and not coupled (deeper inside) magnetite layers in the magnetite, we use the quantitative XMCD and XMLD data presented in Figs. 3(a) and 3(b). In this manner, we can precisely define the angles between the spins in the chosen green and gray domains in both Fe_3O_4 and NiO layers. The quantitative extracted data from the green domains in Fig. 3(a) show a XMCD signal with values ranging from 0.12 to 0.09 whereas the gray domains show a XMCD signal going from 0.09 to 0.06. Given the polarization dependence of Fe L_3 in Fig. 2 the angle between green and gray domains is estimated to $60 \pm 10°$ at $T < T_N$. The quantitative data corresponding to the NiO image in Fig. 3(b) show in the green domains a XMLD value R in the range 1.15 to 1.06 and in the gray domains between 1.03 and 0.92. That leads also to an angle of $60 \pm 10°$ between the two degenerated spins. We can conclude thus that the angular deviation shows the same amplitude in the FM and AF system. This excludes the possibility of averaging signals from different magnetite layers. We can safely conclude that the electron probing depth at the Fe L_3 edge is smaller or equal to the magnetic coupling depth between $NiO/Fe_3O_4(001)$. As will be discussed in detail in the last section, we can estimate for magnetite, that the mean-free path of secondary electrons is $\lambda_e = 1$ nm.[31] In conclusion, we can deduce from our analysis that the magnetic exchange coupling between the FM and the AF layers acts into the magnetite almost up to 1 nm deep.

Moreover, comparing the nanometer FM domains in $Fe_3O_4(001)$ to the nanometer AF domains in NiO in the selected area of Figs. 3(a) and 3(b), we find a coherent matching of all domains as well as a parallel coupling between the FM and the AF spins close to the interface. At low temperatures, the bilayer thus shows a magnetic configuration where alternating magnetic domains result from the competition between two different easy axes in $Fe_3O_4(001)$ and NiO. Above T_N, the magnetic coupling between NiO and $Fe_3O_4(001)$ vanishes completely and the magnetic domain configuration in $Fe_3O_4(001)$ shows more homogenous magnetic domains with spins pointing mainly along the two equivalent in-plane $\langle 100 \rangle$ directions.

B. Statistic analysis of the nanometer domain structures at $T < T_N$

In order to analyze a single magnetic domain as shown in Fig. 4(a), we applied a magnetic field along the [010] direction to saturate $Fe_3O_4(001)$. We analyze at the Fe L_3 edge a magnetic contrast image [Fig. 4(a)] obtained in the geometry shown on the left side. The scale of the magnetic image is 3.8×3 μm^2. The nanometer magnetic domain structure in $Fe_3O_4(001)$ [Fig. 4(a)] shows a homogenous dark background with gray structures. The color code for the specific magnetic image on Fig. 4(a) is given at the right side and corresponds to the general color scale defined in Fig. 1. Here the gray scale is reduced due to the restricted number of domains. In remanence the situation is similar to the previous multidomain configuration but shows now only two

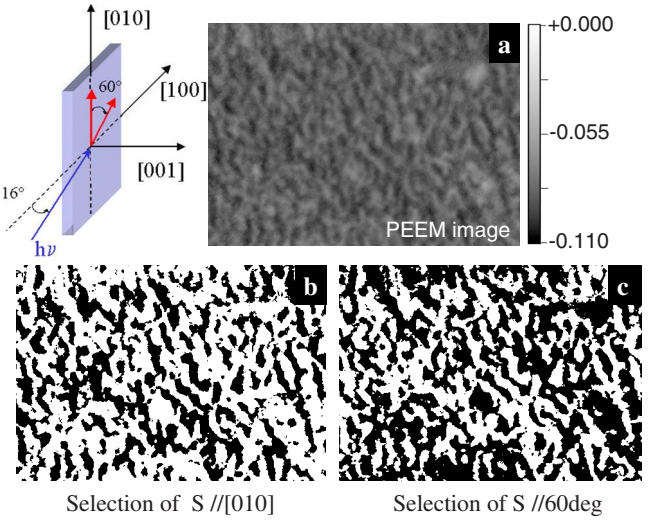

FIG. 4. (Color online) Magnetic contrast image obtained by XMCD-PEEM at the Fe L_3 edge in remanence at $T = 245$ K. (a) The magnetic contrast image shown was rotated by −60° compared to the previous images. The scale of the image is 3.8×3 μm^2. The orientations of the x-ray beam and of the in-plane [010] direction are shown on the left side. (b) The white color selects the domains from Fig. 4(a) with spins parallel to [010]. (c) The white color selects the domains from Fig. 4(a) with spins parallel to 60° off. Only two magnetic domains where the spins are either aligned parallel to [010] (b) or 60° off (c) are present in the magnetic image representing, respectively, 48% and 42% of the total surface. Defects represent 10% of the analyzed surface.

types of domains (∥[010] and +60° off). The background (dark) defines spins oriented 60° from the [010]. The gray structures define spins parallel to [010]. The dark magnetic domains in Fig. 4(a) nearly disappear at T_N, confirming the absence of magnetic coupling with NiO.

The two images presented in Figs. 4(b) and 4(c) correspond to the same area as Fig. 4(a) but now we selected in white the two types of degenerated magnetic domains in order to point out the size and the surface proportions. In particular, the white selected domains in Fig. 4(b) are defined by the XMCD signal going from 0.00 to −0.061 and correspond to the spin direction∥[010]. In Fig. 4(c) the white selected domains are defined by the XMCD signal going from −0.062 to −0.110 and correspond to spins rotated by 60° from the [010] direction. Both spin directions are represented by red arrows in the sketch and are oriented in the surface plane. Counting the pixels corresponding to the white surfaces of Figs. 4(b) and 4(c) we were able to determine the relative surface proportions of both magnetic domains. The quantitative analysis performed thus, allows us to attribute the gray domains [white color in Fig. 4(b)] to 48% and the dark domains [white color in Fig. 4(c)] to 42% of the total surface. The residual 10% could be attributed to the presence of defects. This configuration is similar to the one observed on Fe/NiO/Fe(100) by Rougemaille *et al.*[32] and is attributed to the result of the competition between AF and FM exchange interactions. The typical size of the domains is 70×300 nm^2. A similar exchange-coupling energy can thus be expected in our system. This suggests that the magnetic cou-

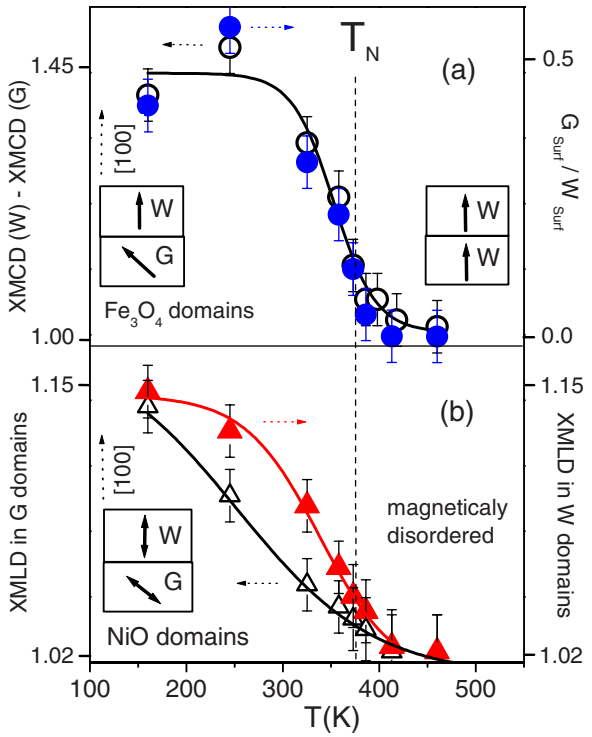

FIG. 5. (Color online) (a) Evolution of the magnetic XMCD contrast differences between *W* and *G* domains inside the nm-sized Fe_3O_4 domains as a function of the temperature (black open circles—left axis). Temperature dependence of the surface ratio W/G in the Fe_3O_4 domains as observed inside the rectangular area in Fig. 3 (blue circles—right axis). (b) The AF order in the NiO film is represented for the *W* (red triangles) and *G* (open triangles) domains. A faster decay of the magnetic order occurs in the *G* domains compared to the *W* domains. The estimated Néel temperature (T_N) for the NiO film is $T_N=375$ K.

pling and the anisotropy in $NiO/Fe_3O_4(001)$ behave very much as they do in Fe/NiO/Fe(001).

C. Local quantitative analysis of the nanometer domains near $T=T_N$

Exploiting quantitatively the magnetic contrast images as a function of the temperature allows to define T_N for the NiO thin film and to compare the individual evolution of the spins in $Fe_3O_4(001)$ and NiO. In order to do this, we analyze quantitatively the histogram obtained in a large micrometer magnetic domain by selecting the gray (*G*) domains and the white domains (*W*) of the magnetic contrast images as a function of the temperature. This is done using the multidomain configuration images as shown in Fig. 1. For the NiO film, we thus measure the magnetic order inside the gray (*G*) domains and white domains (*W*), which are given by the XMLD values *R*. These quantities are reported in Fig. 5(b). In order to analyze the $Fe_3O_4(001)$ data, we report two different quantities. The first consists in the surface proportion of *G* domains normalized to the surface of *W* domains (G_{surf}/W_{surf}) inside a large micrometer magnetic domain. The second consists in the contrast observed between the *W* and *G* domains (*G* domains are characterized by changing XMCD values with temperature) obtained by analyzing the line profile for consecutive nanometer domains. The values are given in XMCD differences between the *W* and *G* domains. These two quantities are reported in Fig. 5(a), respectively, on the right and left axis. Finally, in Fig. 5(b) we observe that, for NiO, the magnetic order in both *W* and *G* domains show continuously decreasing signals as a function of the temperature, completely vanishing at $T=450$ K. Moreover, a residual contribution of XMLD and XMCD contrasts is observed in both layers AF and FM and extend as a tail between 370 and 450 K. Comparing with the temperature dependence of thin NiO/MgO(100) films of Alders *et al.*[33] the tail in our FM/AF coupled NiO film show a significant difference after $T\sim370$ K. This specific phase transition can be tentatively explained by strong inhomogenities of the nanometer domains related to the morphology of the ultrathin NiO film. But a more realistic explication can be given considering exchange and spin-spin correlations in the FM/AF system. Previous results of Scherz *et al.*[34] show that in Co/Cu/Ni trilayers a similar pseudophase transition exists. The static exchange field acting between the two magnetic layers has been shown not to be sufficient to explain the tail of the temperature-dependent magnetization $M(T)$ near T_C(Ni). Higher-order spin-spin correlation seems to be important to account for the tail of $M(T)$ in the trilayers system. Theoretical calculations has to be performed for $NiO/Fe_3O_4(100)$ in order to confirm such a intrinsic effect and exclude interface- and film-morphology effects.

We will now show that the magnetically disordered state in the NiO film is obtained for $T=T_N=370$ K. Starting from low temperatures the AF/FM coupled $Fe_3O_4(001)$ substrate shows a nanometer magnetic-domain pattern labeled *G* (gray contrast). In $Fe_3O_4(001)$, the domains present a continuous rotation of the spin direction toward [100] during the temperature increase, and are thus transformed into magnetic domains labeled *W* (white contrast) as observed in Fig. 5(a). Similar results are obtained by plotting the proportion of *G* surfaces [right axis in Fig. 5(a)] and the magnetic contrast between *W* and *G* [left axis in Fig. 5(a)]. The magnetic transition is found to occur at $T=370$ K in the $Fe_3O_4(001)$ FM domains. The magnetic contrast of the superimposed nanometer domains in Fe_3O_4 changes with temperature in lockstep with the AF contrast observed in NiO, indicating a magnetic exchange coupling at $T<T_N$.

Now, comparing the temperature variation in the FM and AF layers, we can observe a coherent decrease in the signal stemming from the *W* domains in NiO and in $Fe_3O_4(001)$. The *W* domains in NiO are defined by the spins parallel to the orientation of the spins in FM $Fe_3O_4(001)$, so that the exchange interaction favors magnetic order along this direction. Moreover, a specific behavior is observed for the *G* domains in NiO showing a faster decrease with temperature than the *W* domains of NiO. The disordered magnetic state is obtained simultaneously in both nanometer domains. In Fig. 5(b) we observe that, for the NiO film, less thermal activation energy is needed to disorder the spin structure in the *G* domains with respect to the *W* domains. This difference can be explained by supposing that the *G* domains in NiO show locally a reduced exchange coupling with the $Fe_3O_4(001)$ domains. We clearly observe in Fig. 5(b) that the local dif-

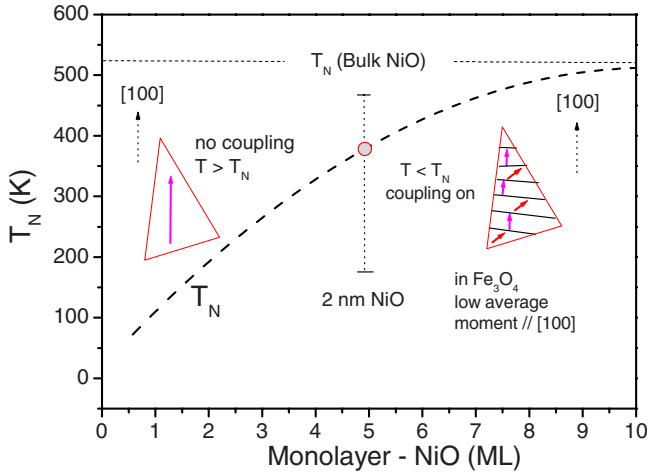

FIG. 6. (Color online) Diagram where we plot schematically T_N as a function of the NiO film thickness corresponding to the value extracted from this work and converging toward the value of bulk NiO. The film studied here is marked as a circle corresponding to the thickness of 2 nm (5 ML) and which is now defined by a Néel temperature $T_N=373$ K. The temperature range studied in our work is indicated as vertical dots. The magnetic microstructures are represented as observed in our experiment, below and above T_N. The transition from the single micrometer-sized domains to a twofold degenerated nanometer domain configuration is possible as a function of the temperature or NiO film thickness.

ference consists in a modification of the slope of the magnetic order versus temperature in the NiO film (G domains) whereas T_N is not affected.

Interestingly, the macroscopic average magnetic moment measured at the Fe $L_{2,3}$ edges along the [100] direction would show a lower value at $T<T_N$ compared to the one at $T>T_N$ because of the presence of gray domains with tilted spins. By the simple fact that magnetic coupling exists, the microstructure of the magnetic domains produces a strong reduction in the magnetic moment in $Fe_3O_4(100)$. In coupled $NiO/Fe_3O_4(100)$ this happens without any chemical mixing or uncompensated spins as often demonstrated at such interfaces.[20,26,27] Especially, the presence of a spinel $NiFe_2O_4$ at the interface has been interpreted as the unique factor responsible for reduced magnetic moments in multilayers or thin films. The estimation of the reduction in the average magnetic moment is provided by the proportion of spins parallel to 60° which amounts to 45% (Fig. 4). In a single micrometer domain, the average magnetic moment along [100] should thus be reduced by 25% at $T<T_N$. Moreover, the macroscopic magnetic moment measured in remanence should also show the reduction in the moments at low temperatures. This is qualitatively what is observed comparing the hysteresis between clean $Fe_3O_4(100)$ and ultrathin $NiO/Fe_3O_4(100)$ films grown in the same conditions and observed by XMCD at the Fe L_3 edge at $T=200$ K.[20]

The consequence of the presence of such magnetic microstructures in coupled ultrathin $NiO/Fe_3O_4(001)$ is shown in Fig. 6 where we schematically plot the evolution of T_N as a function of the NiO film thickness. The film studied here is marked by a circle corresponding to the thickness of 2 nm (5 ML) and to $T=T_N=373$ K. The temperature range studied here is indicated by vertical dots. The magnetic microstructures observed in our experiment below and above T_N are drawn as insets. Figure 6 shows clearly that, when measuring at one single temperature, for instance at room temperature ($T=300$ K), increasing NiO thicknesses must lead to a transition from the single micrometer-sized domains to a twofold degenerated nanometer domain configuration resulting in a lower macroscopic moment in $Fe_3O_4(001)$. Hence, we can conclude that the lowering of the magnetic moment could be a simple consequence of the magnetically decoupled-coupled transition of the $NiO/Fe_3O_4(001)$ system. Thus, we can tentatively explain the results obtained by XMCD-PEEM from I. P. Krug *et al.*,[28] for instance, where magnetic moments where measured in the micrometer scale at room temperature and for different NiO thicknesses. The NiO thickness threshold where decreasing averaged magnetic moments where observed, would be consistent with the appearance of AF order in the NiO film ($T_N=300$ K) inducing a degenerated magnetic configuration at the nanometer scale.

IV. DISCUSSION

The accurate analysis of the magnetic domains in the $NiO/Fe_3O_4(001)$ bilayer below and above T_N provides a detailed description of the micromagnetic configuration of coupled FM/AF layers and allows to associate them with specific coupling mechanism. We show that there are two different length scales in $Fe_3O_4(001)$ domains which are located close to the interface. On the micrometer scale, large domain configurations can be observed in $Fe_3O_4(001)$ above T_N. These are supposed to spread over the entire magnetite substrate connected to structure and defects in $Fe_3O_4(001)$ but here we observe theme close to the interface (~1 nm) due to the detection technique.

The training effects observed on the magnetic domains in magnetite are observed after an excursion at the Néel temperature of NiO. These link the effects to the presence of the exchange-coupled AF NiO film rather than to defects in the magnetite. As suggested by Binek,[30] at the FM/AF interface, the AF pinning layers can be considered as unstable, considering the magnetization. As the temperature increases the magnetic configuration at the interface of NiO can reach a new and more stable configuration, favored by total-energy considerations. The switching of the magnetic defects in the AF film at $T>T_N$ has thus to be considered in combination with the exchange coupling between $Fe_3O_4(001)$ and NiO (acting at $T<T_N$) in order to explain the training effects observed in the magnetite.

The nanometer domains observed at $T<T_N$ originate directly from the magnetic exchange coupling at the AF/FM interface as pointed out by their vanishing at $T>T_N$. The modification of the magnetic fine structure observed at $T=150$ K after each excursion to $T>T_N$ suggests that the configuration of the nanometer-sized domains is probably related mainly to exchange-coupling energy of the AF/FM interface, rather than to the pinning of the magnetic domains on the structural defects as suspected for the magnetite micrometer-sized domains observed at $T>T_N$.

We have shown that the angular deviation of 60° observed below T_N is identical in both FM and AF layers. This sug-

gests that the magnetic exchange coupling depth is almost as large as the electron probing depth at the Fe L_3 edge. The exact definition of the probing depth in magnetite led to some controversy in the past few years. A primary study given by S. Gota *et al.*[35] showed that the absorption spectra of the magnetite, recorded in the total-electron yield mode, exhibit strong saturation effects. They evaluated both the probing depth of the electrons and the absorption length at the FeL_3 and FeL_2 edges for the iron oxide by fitting the magnetite thickness dependent intensities at the FeL_3 and FeL_2 edges. Comparing with the transition metals, where Nakajima *et al.*[36] estimated the probing depth to 1.7 nm for Fe, 2.0 nm for Co, and 2.5 nm for Ni, the magnetite probing depth of 4.5 nm was surprisingly high but coherent with the low iron density in magnetite. Following works by Huang *et al.*[37] and Pilard *et al.*[20] showed both large spin and orbital magnetic moments for magnetite using the previously defined probing depth of 4.5 nm, in order to correct for saturation effects present in the total-electron yield detection mode. In opposite to this work, Goering *et al.* suggested a value of $\lambda_e = 1$ nm (Ref. 31) for the probing depth. They have normalized the XAS and XMCD data in order to correct for the saturation effects using this smaller value. A large-spin magnetic moment and a quenched orbital magnetic moment were thus extracted. More recently Kallmayer *et al.*[38] published experiments performed in the transmission detection mode free from saturation effects and confirmed that the electron probing depth indeed is close to 1 nm. Thus, the magnetic exchange-coupling depth of the AF NiO thin film into the 60-nm-thick FM $Fe_3O_4(001)$ substrate is of almost 1 nm. We give thus here a value for the exchange-coupling length into magnetite found in the literature, since the exact value cannot be directly extracted from our X-PEEM measurements. In any case whatever the length is, it is largely below the total magnetite thickness of 60 nm and ensures the localized character of the interface magnetic exchange coupling.

In each nanometer domain we confirm a parallel orientation between the NiO and $Fe_3O_4(001)$ spins coupled with the interface compound formed at $NiO/Fe_3O_4(001)$ favoring parallel coupling as shown in our previous work.[20] The magnetic coupling at $T < T_N$ favors the nanometer structuration into a twofold degenerated domain pattern. Thus the parallel coupling induces a configuration where alternating nanometer domains show spins aligned parallel to [100] and to [210], probably resulting from the balance between the preferred spin orientation in $Fe_3O_4(001)(\|[100])$ and the preferred spin directions in $NiO(\|[210])$. Macroscopically, the existence of such a nanometer magnetic-domain pattern in coupled AF/FM layers could be at the origin of the absence of any macroscopic exchange bias in this system. More precisely, the macroscopic magnetic measurements give generally means values over the degenerated spin configurations in the nanometer range, characterized by different exchange-coupling energies. The individual nanometer magnetic domains therefore do not lead to a single and common energy shift in the magnetization curve.

The micromagnetic configuration evidenced in this work show that NiO spins can be oriented parallel to [210] or to [100]. The inhomogenous spin orientation of the NiO films show that the magnetocrystalline effect (arising from the misfit strain in NiO, assumed homogenous) which was claimed to explain a collinear coupling of the NiO spins with the $Fe_3O_4(001)$ spin direction (in-plane $\langle 100 \rangle$)[20] is not the dominant factor governing the magnetic state. The results rather show a more complex configuration where magnetoelastic energy is associated with exchange contribution arising from each FM and AF layers reducing the local dipolar moments in the $Fe_3O_4(001)$ micrometer domains. This final energy balance defining the micromagnetic domain structures should be NiO thickness dependent.

V. CONCLUSIONS

Using the X-PEEM technique we have been able to experimentally describe the magnetic-domain patterns at the $NiO/Fe_3O_4(001)$ interface confirming a parallel coupling between the NiO and $Fe_3O_4(001)$ spins. We determine the Néel temperature of $T_N = 375$ K for the ultrathin 2 nm NiO film. The magnetic coupling at $T < T_N$ favors a magnetic configuration in the nanometer scale where a twofold degenerated domain pattern can be achieved in each micrometer magnetic domain. Thus, the magnetic parallel coupling is characterized by alternating nanometer domains where the spins are aligned parallel to [100] and to [210]. The micromagnetic configuration shows that the NiO and $Fe_3O_4(001)$ bilayer develops a complex configuration were magnetoelastic energy is associated with exchange contribution arising from each FM and AF layers. This energy balance defining the micromagnetic-domain structures should be NiO thickness dependent.

ACKNOWLEDGMENTS

The authors thank Salia Cherifi and Laurent Ranno for providing the oxide substrates. This work was supported by the E.U. Contract Integrated Infrastructure Initiative I3 in FP6-Project No. R II 3 CT-2004-506008, BESSY IA-SFS Access Programme.

*Corresponding author; Present address: IPCMS–GSI, 23, rue du Loess, F-67037 Strasbourg Cedex 02, France. FAX: (+33) 3 88 10 72 48; christine.boeglin@ipcms.u-strasbg.fr

[1] A. E. Berkowitz and Kentaro Takano, J. Magn. Magn. Mater. **200**, 552 (1999).
[2] H.-J. Freund, H. Kuhlenbeck, and V. Staemmler, Rep. Prog. Phys. **59**, 283 (1996).
[3] G. Renaud, Surf. Sci. Rep. **32**, 1 (1998).
[4] H. L. Meyerheim, R. Popescu, N. Jedrecy, M. Vedpathak, M. Sauvage-Simkin, R. Pinchaux, B. Heinrich, and J. Kirschner, Phys. Rev. B **65**, 144433 (2002).
[5] H.-J. Freund, Surf. Sci. **500**, 271 (2002).

[6] H. T. Jeng and G. Y. Guo, Phys. Rev. B **65**, 094429 (2002).
[7] C. Cheng, Phys. Rev. B **71**, 052401 (2005).
[8] Y. S. Dedkov, M. Fonin, D. V. Vyalikh, J. O. Hauch, S. L. Molodtsov, U. Rudiger, and G. Guntherodt, Phys. Rev. B **70**, 073405 (2004).
[9] Y. S. Dedkov, U. Rudiger, and G. Guntherodt, Phys. Rev. B **65**, 064417 (2002).
[10] H. J. Kim, J. H. Park, and E. Vescovo, Phys. Rev. B **61**, 15288 (2000).
[11] C. A. Ventrice, Jr., Th. Bertrams, H. Hannemann, A. Brodde, and H. Neddermeyer, Phys. Rev. B **49**, 5773 (1994).
[12] C. Mocuta, A. Barbier, G. Renaud, Y. Samson, and M. Noblet, J. Magn. Magn. Mater. **211**, 283 (2000); A. Barbier, C. Mocuta, H. Kuhlenbeck, K. F. Peters, B. Richter, and G. Renaud, Phys. Rev. Lett. **84**, 2897 (2000).
[13] R. S. Saiki, A. P. Kaduwela, J. Osterwalder, C. S. Fadley, and C. R. Brundle, Phys. Rev. B **40**, 1586 (1989).
[14] J. A. Borchers, R. W. Erwin, S. D. Berry, D. M. Lind, J. F. Ankner, E. Lochner, K. A. Shaw, and D. Hilton, Phys. Rev. B **51**, 8276 (1995).
[15] Y. Ijiri, J. A. Borchers, R. W. Erwin, S. H. Lee, P. J. van der Zaag, and R. M. Wolf, Phys. Rev. Lett. **80**, 608 (1998).
[16] S. I. Csiszar, M. W. Haverkort, Z. Hu, A. Tanaka, H. H. Hsieh, H. J. Lin, C. T. Chen, T. Hibma, and L. H. Tjeng, Phys. Rev. Lett. **95**, 187205 (2005).
[17] H. Ohldag, A. Scholl, F. Nolting, S. Anders, F. U. Hillebrecht, and J. Stohr, Phys. Rev. Lett. **86**, 2878 (2001).
[18] H. Ohldag, T. G. Regan, J. Stohr, A. Scholl, F. Nolting, J. Luning, C. Stamm, S. Anders, and R. L. White, Phys. Rev. Lett. **87**, 247201 (2001).
[19] S. Stanescu, C. Boeglin, A. Barbier, and J. P. Deville, Surf. Sci. **549**, 172 (2004)
[20] M. Pilard, O. Ersen, S. Cherifi, B. Carvello, L. Robian, B. Muller, F. Scheurer, L. Ranno, and C. Boeglin, Phys. Rev. B **76**, 214436 (2007).
[21] M. Finazzi, Phys. Rev. B **69**, 064405 (2004).
[22] S. Stanescu, C. Boeglin, A. Barbier, and J. P. Deville, Phys. Rev. B **67**, 035419 (2003).
[23] T. J. Regan, H. Ohldag, C. Stamm, F. Nolting, J. Luning, J. Stohr, and R. L. White, Phys. Rev. B **64**, 214422 (2001).
[24] M. Finazzi, A. Bambrilla, L. Duo, G. Ghiringhelli, M. Portalupi, F. Ciccacci, M. Zacchigna, and M. Zangrando, Phys. Rev. B **70**, 235420 (2004).
[25] M. Marre and H. Neddermeyer, Surf. Sci. **287**, 995 (1993), S. D. Peacor and T. Hibma, *ibid.* **301**, 11 (1994).
[26] R. F. C. Farrow, M. J. Carey, R. F. Marks, P. M. Rice, and D. J. Smith, Appl. Phys. Lett. **77**, 1191 (2000).
[27] C. Gatel, E. Snoeck, V. Serin, and A. Fert, Eur. Phys. J. B **45**, 157 (2005).
[28] I. P. Krug, F. U. Hillebrecht, H. Gomonaj, M. W. Haverkort, A. Tanaka, L. H. Tjeng, and C. M. Schneider, EPL **81**, 17005 (2008); I. P. Krug, F. U. Hillebrecht, W. Haverkort, A. Tanaka, L. H. Tjeng, H. Gomonay, A. Fraile-Rodriguez, F. Nolting, S. Cramm, and C. M. Schneider, Phys. Rev. B **78**, 064427 (2008).
[29] E. Arenholz, G. van der Laan, R. V. Chopdekar, and Y. Suzuki, Phys. Rev. Lett. **98**, 197201 (2007).
[30] C. Binek, Xi He, and S. Polisetty, Phys. Rev. B **72**, 054408 (2005).
[31] E. Goering, S. Gold, M. Lafkioti, and G. Schütz, EPL **73**, 97 (2006).
[32] N. Rougemaille, M. Portalupi, A. Brambilla, P. Biagioni, A. Lanzara, M. Finazzi, A. K. Schmid, and L. Duò, Phys. Rev. B **76**, 214425 (2007).
[33] D. Alders, L. H. Tjeng, F. C. Voogt, T. Hibma, G. A. Sawatzky, C. T. Chen, J. Vogel, M. Sacchi, and S. Iacobucci, Phys. Rev. B **57**, 11623 (1998).
[34] A. Scherz, C. Sorg, M. Bernien, N. Ponpandian, K. Baberschke, H. Wende, and P. J. Jensen, Phys. Rev. B **72**, 054447 (2005).
[35] S. Gota, M. Gautier-Soyer, and M. Sacchi, Phys. Rev. B **62**, 4187 (2000).
[36] R. Nakajima, J. Stöhr, and Y. U. Idzerda, Phys. Rev. B **59**, 6421 (1999).
[37] D. J. Huang, C. F. Chang, H. T. Jeng, G. Y. Guo, H. J. Lin, W. B. Wu, H. C. Ku, A. Fujimori, Y. Takahashi, and C. T. Chen, Phys. Rev. Lett. **93**, 077204 (2004); D. J. Huang, C. F. Chang, J. Chen, H. J. Lin, S. C. Chung, H.-T. Jeng, G. Y. Guo, W. B. Wu, S. G. Shyu, and C. T. Chen, J. Electron Spectrosc. Relat. Phenom. **137–140**, 633 (2004).
[38] M. Kallmayer, K. Hild, H. J. Elmers, S. K. Arora, Han-Chun Wu, R. G. S. Sofin, and I. V. Shvets, J. Appl. Phys. **103**, 07D715 (2008).